Inverse reconstruction techniques and their applicability for acoustic travel-time tomography

G. Fischer, M. Barth and A. Ziemann

Universität Leipzig, Institut für Meteorologie, D - 04103 Leipzig, Germany, e-mail: gfischer@uni-leipzig.de

Introduction

In the last decades the feasibility of acoustic travel-time tomography in the atmospheric boundary layer has been successfully demonstrated in a variety of numerical and experimental studies [1]-[3]. Therefore, travel-time measurements of propagating sound signals along known sound ray paths between several transmitters and receivers have been inverted to estimate the effective sound speed field of an analyzed medium. Using the dependency of the sound speed on temperature and wind vector, area-averaged fields of those meteorological quantities can be reconstructed.

The quality of the reconstruction is mainly influenced by the accuracy of the measurements and the inverse reconstruction technique including the reconstruction accuracy of the algorithm itself. Because of the limited number of acoustic sensors which can be arranged around a measurement area the demand for a convenient robust and accurate inverse algorithm is essential. As a result of the variety of existing and applied inverse reconstruction techniques the aim of this study was to determine which inverse algorithm is suited for which special demand, e.g. in the atmosphere. Here, we concentrate on reconstruction of temperature fields. Therefore, based on the same initial travel-time data, we analyzed the results achieved with matrix inversion, simultaneous iterative reconstruction technique, and stochastic inversion regarding their spatial resolution, accuracy and computational efficiency.

Inversion techniques

In a moving atmosphere the measured travel time of a sound signal between a fixed transmitter and a receiver is influenced by the temperature as well as the wind vector along this propagation path. Using the approach to separate these influences on the measured travel times as proposed in [4] the temperature dependent travel time τ can be expressed as

$$\tau = \int_L \frac{\mathrm{d}l}{c_L(T_{av})} \qquad [\mathrm{s}] \qquad (1)$$

where dl is the element of arc length along the propagation path L and c_L indicates the Laplace's sound speed which depends on the acoustic virtual temperature T_{av} [5]. For simplification, the reconstructed acoustic virtual temperature is denoted as temperature in the following.

Assuming straight-line sound propagation in the investigation medium, equation (1) can be linearized [6]. Furthermore, in practice, only a limited number of acoustic sensors is available. Thus, the finite number of travel times leads to the limitation that only discrete temperature distributions can be reconstructed. Here, a discretization approach is used which divided the tomographic array into J squared grid cells with a finite size. Inside these cells the reconstructed values are assumed to be constant.

After linearization and discretization of equation (1) the different inverse algorithms solve the resulting system of linear equations in a different manner. The matrix inversion (MI) and simultaneous iterative reconstruction technique (SIRT), which are based on the method of least squares, minimize the sum of quadratic differences between the reconstructed and the measured travel times. Both techniques require the investigation area to be divided into grid cells of constant size. In most cases the number of sound rays is not equal to the number of grid cells, thus leading to an under-determined equation system. To resolve this problem for an MI approach, a singular value decomposition scheme is utilized [7], whereas SIRT determines the searched distribution with an iterative approximation (see [2] for details). SIRT is characterized as a method with satisfactory convergence and stability properties as well as simple handling, especially during online evaluation. During one iteration step the here used SIRT method first considers all travel times before adding a weighted travel-time correction to the previous sound speed within each grid cell [4].

In contrast to those inverse techniques the stochastic inversion (SI) approach minimizes each individual difference between the reconstructed and the real sound speed. Therefore, additional information about the investigation area, such as turbulence parameters to describe the correlation between measurements and model parameters [1], is required. Unlike the other two groups of inverse techniques, the temperature fields reconstructed by SI are composed of a mean temperature value for the whole investigation area, which is calculated in a first step, and spatial temperature fluctuations at discrete points within the area. To facilitate the comparability between the individual reconstruction techniques, the area of investigation is also subdivided into squared cells for SI. The temperature fluctuations are reconstructed for the centres of these cells and assumed to be constant for the whole cell.

Analysis of synthetic data

The generation of synthetic travel times requires the presetting of a measurement geometry and initial temperature distributions within the investigation area. Thereby, the quality of the reconstructed fields depends on the number and the arrangement of the acoustic sensors. For

the numerical study, a square field with 2.0 m base length and a combination of 8 transmitters and 8 receivers as well as 16 transmitters and 16 receivers was chosen. For real measurements in the atmospheric boundary layer transmitter-receiver pairs have to be arranged in such a way that the influence of temperature and wind speed on the measured sound speed can be separated using bidirectional sound ray paths [4]. The resulting arrangement for the 8 transmitter-receiver pairs and the corresponding 64 sound ray paths is illustrated in Figure 1. The reconstruction of a temperature field with MI and SIRT is only possible when the number of sound rays is equal or greater then the number of grid cells and every cell is passed by at least one sound ray. Therefore, the test field was subdivided into cells with (0.4×0.4) m^2 of size.

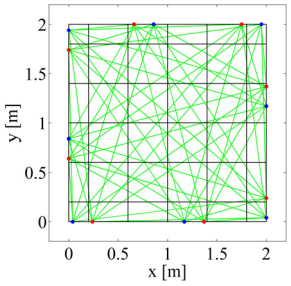

Figure 1: Setup of 8 transmitters (red circles) and 8 receivers (blue circles) used for numerical sensitivity studies. For tomography, the array is subdivided into (0.4×0.4) m^2 grid cells (black lines) which are crossed by 64 different sound ray paths (green lines).

In a next step, several types of temperature distributions were converted into Laplace's sound speed fields. Finally, the desired data sets of synthetic travel times for each distribution could be determined with the help of the well-known positions of transmitters and receivers. For one type, the temperature was varied continuously in x- or y-direction inside the measurement field (type: 'gradient'). Other data sets based on homogeneous temperature fields, which were superposed by locally colder or warmer Gaussian inhomogeneities in the centre or corner of the testing area (type: 'centre', 'corner').

In the following, an example of the latter type is discussed. Here, a constant background field of 15 °C was superposed with an inhomogeneity in the left corner of the investigation area as drawn in Figure 2a. This inhomogeneity is characterized by a maximum temperature change of 1 K. The spatial resolution was adapted to the test field shown in Figure 1. Furthermore, the resulting data was used as input for the tomographic reconstruction algorithms. The reconstructed temperature distributions of the initial travel-time data of Figure 2a are demonstrated in Figure 2b for MI, in Figure 2c for SIRT, and in Figure 2d for SI, respectively. The comparison of the original and reconstructed fields shows that all inverse techniques reconstructed the structure of the temperature field with a good accuracy. The errors of the temperature values within the grid cells were less than 0.2 K. The largest temperature differences occur in the area of the inhomogeneity and at the borders of the tomographic grid due to the lower number of sound rays in the smaller boundary cells. A more detailed analysis shows that MI often produces tessellate structures, whereas reconstructions with SIRT produce only weak structures of that kind. In tomograms reconstructed with SI such artefacts were never observed. This holds for the discussed example, as well as all other mentioned types of temperature distributions.

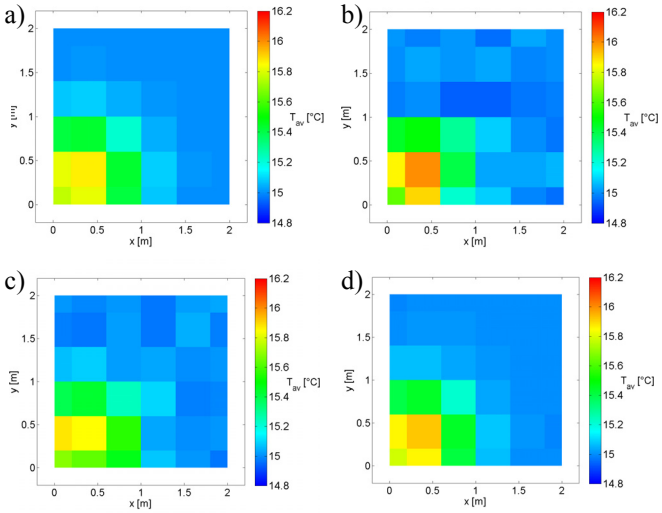

Figure 2: a) Simulated distribution of the acoustic virtual temperature of type 'corner' with a spatial resolution of (0.4×0.4) m^2. Temperature distribution was reconstructed with matrix inversion (b), SIRT (c), and stochastic inversion (d), respectively.

The deviation between the reconstructed and the simulated temperature field is a convenient parameter to determine the quality of the reconstructed area-averaged temperature field for each inverse algorithm. Note that reconstruction accuracy also depends on the spatial resolution of the reconstructed quantities, which is influenced by the number of acoustic sensors and the distribution of the sound rays in the test area. Therefore, according to [8] the Euclidic distance *ED* is considered:

$$ED = \frac{1}{J}\sum_{j=1}^{J}\left(c_{j,sim} - c_{j,reconstr}\right)^2 \qquad [\mathrm{m^2 s^{-2}}] \qquad (2)$$

J denotes the total number of grid cells. The *ED* value is only available for numerical sensitivity studies, because it characterizes the similarity between the (known) simulated Laplace's sound speed $c_{j,sim}$ and the reconstructed sound speed $c_{j,reconstr}$ in grid cell j. Obviously, the inversion results become better for smaller *ED* values.

The *ED* values of the reconstructed temperature fields shown in Figure 2 (b-d) for 8 as well as 16 transmitter-receiver pairs (64 and 256 sound rays) are compiled in Table 1. The averaged values of MI are greater than those for SIRT and SI. By doubling the number of acoustic sensors around the investigation area a considerable error reduction for MI and SIRT could be obtained whereas the results of SI remain constant.

Similar results were achieved with different spatial resolutions and other underlying temperature distributions. In conclusion, the algorithm MI calculated temperature fields with the largest errors whereas SI produced the smallest. Thus, SIRT and SI are preferred because of yielding the most stable reconstruction results.

ED $[10^{-3}m^2s^{-2}]$	Reconstruction technique		
	MI	SIRT	SI
64 sound rays	1.39	0.76	0.08
256 sound rays	0.38	0.13	0.08

Table 1: Calculated ED values for the three reconstruction techniques for the simulation type 'corner'. The resolution of the tomographic area was (0.4 × 0.4) m^2.

Another aspect when comparing the inverse algorithms is their applicability to provide the searched quantities in reasonable time with low computational effort. In particular, this plays an import role for online data evaluation during measurement campaigns or for operational control of processes, e.g. to regulate the temperature in a medium within a certain range. Some mean computing times for the chosen resolution of (0.4 × 0.4) m^2 can be found in Table 2. The MI algorithm has the shortest reconstruction time followed by SIRT. By contrast, the SI algorithm requires an increased storage capacity and has a relatively high computational time. This is mainly because of the high amount of calculation steps for the determination of the correlation data. Moreover, a doubling of the number of sensors along the investigation area produces an increasing computational time of about 10 % for all algorithms.

Computing time [s]	Reconstruction technique		
	MI	SIRT	SI
64 sound rays	0.002	0.008	50
256 sound rays	0.003	0.05	800

Table 2: Average required computing time for the three inverse algorithms obtained with a MATLAB routine on a Pentium 4 Desktop PC (3.20 GHz CPU, 2 GB RAM) for a resolution of the tomographic area of (0.4 × 0.4) m^2.

Hence, in combination with the previous numerical results, the SIRT algorithm is preferred for measurement campaigns with online analysis, since this inverse technique yields quickly stable reconstruction results with reasonable accuracy.

Analysis of experimental data

For the verification of the reconstruction results obtained by numerical experiments a laboratory measurement was carried out. Sensitivity tests with experimental data allow a first evaluation of the three inverse algorithms concerning their applicability under atmospheric conditions.

Similar to the numerical studies, 8 transmitter-receiver pairs were arranged along the (1.23 × 1.23) m^2 portable laboratory system. The distribution of the sound rays and the grid cells with a size of (0.3 × 0.3) m^2 is illustrated in Figure 3. Moreover, the setup includes a circular heating plate positioned below grid cell 14, which is marked in Figure 3. The powered heating plate creates a temperature inhomogeneity analogous to that used for the numerical sensitivity studies.

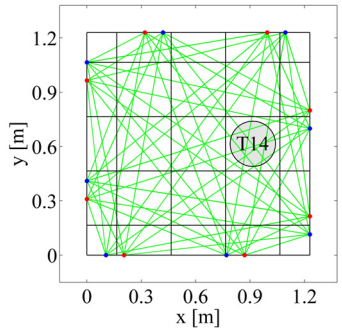

Figure 3: Setup for the experimental study. The green lines denote the sound rays between the 8 transmitter-receiver pairs (red and blue circles, respectively) passing the grid cells (black lines) with a dimension of (0.3 × 0.3) m^2. A heating plate (grey circle) was placed below grid cell 14.

Using the cross correlation of the sent and received signals the travel times of acoustic signals between the defined positions of the transmitters and the receivers could be determined. The characteristics of the acoustic signals being applied here are described in [4]. Due to the relatively short sound ray distances in the investigation area, inaccurate measurements of the travel times and of the device positions result in high uncertainties of the reconstructed distribution. Therefore, it is favourable to measure changes of temperature relative to a well known reference state. The experiment starts with three initial measurements at constant conditions. Afterwards, the heating plate was switched on in order to observe the time dependent behaviour of the area-averaged temperature distribution. Reaching a temperature maximum the heating plate was switched off and the temporal cooling process was observed. The repetition rate for a single measurement was 20 s.

In all reconstructed temperature fields the influence of the heating plate was clearly visible. To compare the results of the different inverse techniques, the temporal development of the area-averaged temperature value in the grid cell 14, which was directly influenced by the heating plate, is shown in Figure 4. With an Assmann psychrometer the constant background temperature of 21.8 °C was measured in the laboratory. Approximately 80 s after switching on the heater, all inverse algorithms reconstructed a warming in the observed grid cell. Further on, the temperature increased continuously. Note that the MI approach reconstructs the highest warming and therewith most likely produces reconstruction results with the highest absolute differences between the original and the reconstructed field as predicted by the numerical studies. The reconstructed temperatures with SIRT and SI are more consistent. In comparison with the previous studies, it can be assessed that these both

algorithms determine the temperature differences with the highest quality in the experimental study.

The temporal variations in temperature, which partly exceed 1.0 K, are qualitatively consistent in all inverse techniques. The reason for this process is substantially the generation of warm air bubbles which do not rise continuously from the heating surface. Thus, random thermal eddies cause the fluctuation of the temperature value in cell 14.

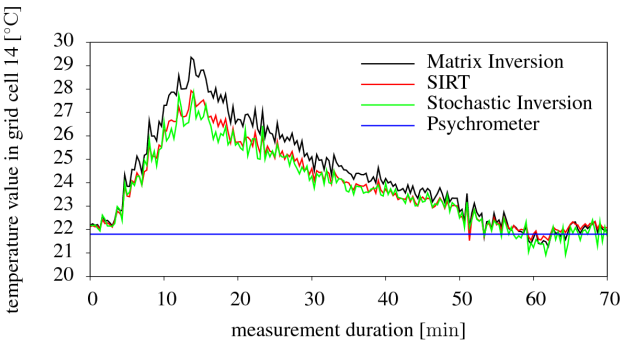

Figure 4: Temporal development of the area-averaged temperature variation within grid cell 14 generated by switching on and off a heating plate under the observed cell. The psychrometer measurement takes place near the tomographic system in about the same height.

Furthermore, Figure 4 shows that with decreasing magnitude of the temperature inhomogeneity caused by switching off the heating plate, the differences between the temperatures from the particular algorithms are also decreased. A similar behaviour was observed in numerical studies. Here, small temperature differences were better reconstructed than larger differences in area under investigation.

Another essential benefit of SI is the ability of visualizing turbulent structures in the temperature field. Here, at the expense of longer computing times, temperature tomograms with a high spatial resolution of (0.01×0.01) m^2 may be calculated as a part of the postprocessing. Figure 5 exemplarily presents the resulting tomogram after 5 min testing time. Obviously, the heating plate is well reproduced in the temperature distribution and other small turbulent structures are visible.

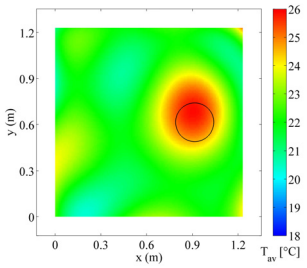

Figure 5: Tomogram of the temperature reconstructed by SI with a spatial resolution of (0.01×0.01) m^2 after 5 min testing time. A heating plate (circle) below the investigation area was switched on.

The results of this study show that all tested inverse techniques are principally applicable for acoustic travel-time tomography of the atmosphere. The best reconstruction results regarding a high spatial resolution and small reconstruction errors were achieved with SI. However, besides long computing times, additional turbulence parameters have to be known. Oppositely, SIRT is preferable for fast online interpretation of the measured data since its reconstruction results are also quite accurate.

Further investigations will concentrate on the comparison of the behaviour of the different algorithms on spatial scales of up to several hundred meters in field studies in the atmospheric boundary layer including the visualisation of turbulent structures. Therefore, the properties of the inverse techniques of the simultaneous reconstruction of area-averaged temperature and wind speed distributions within a tomographic area have to be considered as well.

References

[1] Wilson, D. K., Thomson, D. W.: Acoustic tomographic monitoring of the atmospheric surface-layer. J. Atmos. Ocean. Technol. **11** (1994), 751-769.

[2] Ziemann, A., Arnold, K., Raabe, A.: Acoustic tomography in the atmospheric surface layer. Ann. Geophysicae **17** (1999), 139-148

[3] Vecherin, S. N., Ostashev, V. E., Goedecke, G. H., Wilson, D. K., Voronovich, A. G.: Time-dependent stochastic inversion in acoustic travel-time tomography of the atmosphere. J. Acoust. Soc. Am. **119** (2006), 2579-2588.

[4] Barth, M., Raabe, A., Arnold, K., Resagk, C., Du Puits, R.: Flow field detection using acoustic travel time tomography. Meteorol. Z. **16** (2007), 443-450.

[5] Ostashev, V. E.: Acoustics in Moving Inhomogeneous Media. E & FN Spon, London, 1997.

[6] Ziemann, A., Arnold, K., Raabe, A.: Acoustic tomography as a remote sensing method to investigate the near-surface atmospheric boundary layer in comparison with in situ measurements. J. Atmos. Ocean. Technol. **19** (2002), 1208-1215.

[7] Anderson, E., Bai, Z., Bischof, C., Blackford, S., Demmel, J., Dongarra, J., Du Croz, J., Greenbaum, A., Hammarling, S., McKenney A., Sorensen, D.: LAPACK User's Guide. SIAM, Philadelphia, 1999.

[8] Krajewski, C., Dresen, L., Gelbke, C., Ruter, H.: Iterative tomographic methods to locate seismic low-velocity anomalies - a model study. Geophys. Prosp. **37** (1989), 717-751.